



Repositorio Institucional de la Universidad Autónoma de Madrid

<https://repositorio.uam.es>

Esta es la **versión de autor** del artículo publicado en:

This is an **author produced version** of a paper published in:

Applied Geochemistry 93 (2018): 1-9

DOI: <https://doi.org/10.1016/j.apgeochem.2018.03.012>

Copyright: © 2018 Elsevier Ltd. All rights reserved.

El acceso a la versión del editor puede requerir la suscripción del recurso

Access to the published version may require subscription

Geochemical conditions for the formation of Mg silicates phases in bentonite and implications for radioactive waste disposal

Raúl Fernández¹, Daniel González-Santamaría¹, María Angulo¹, Elena Torres², Ana Isabel Ruiz¹, María Jesús Turrero², Jaime Cuevas¹

¹Department of Geology and Geochemistry, Faculty of Sciences, Autonomous University of Madrid, Cantoblanco, 28049, Madrid, Spain

²CIEMAT, Av. Complutense 40, 28040, Madrid, Spain

Corresponding author: Raúl Fernández

Telephone: +34 91497 4804

Fax: +34 91497 6440

Abstract

The present study evaluates the formation of magnesium silicates phases as a result of the alkaline alteration of FEBEX bentonite in long-term experiments. The results are relevant in the context of radioactive waste disposal since the bentonite barrier will partly change its original mineralogy and condition its long-term geochemical behavior. Bentonite samples from an *in situ* experiment of interaction with a CEM-II-type concrete performed for 13 years in a rock gallery and a laboratory experiment of interaction with a CEM-I-type concrete performed for 10 years provide some experimental evidences on the mineralogical alteration. Results required multiple analytical techniques to resolve the nature of the Mg silicates. X-ray diffraction, thermogravimetric analyses, scanning electron microscopy, infrared spectroscopy and ²⁷Al and ²⁹Si nuclear magnetic resonance have been used. The mineralogical alteration is complex since several Mg silicates may coexist in the same region not only with themselves but also with carbonates and calcium (aluminium) silicate hydrates. Brucite intercalation in the interlayer of smectite, previously reported as a chlorite-like phase in a former study, is observed. In addition, a serpentine-type mineral phase was better observed in the *in situ* samples, at least by XRD, and a 2:1 trioctahedral phyllosilicates was better observed in the laboratory samples. Formation of Mg silicates in the bentonite barrier may buffer the Ca alkaline front originated in concrete and may decrease the porosity at the concrete-bentonite interface.

Keywords: radioactive waste storage; concrete-bentonite interaction; alkaline alteration; magnesium silicates phases.

32

33 **Highlights**

- 34 Long-term concrete-bentonite interaction is studied in long-term experiments
- 35 Mg-silicates precipitated in bentonite at the interface with concrete
- 36 Trioctahedral Mg silicates and serpentine-type minerals are detected
- 37 Brucite intercalation in the interlayer of smectite is also detected
- 38 The Ca alkaline front from concrete is buffered by the Mg silicates formed in bentonite

39 **Introduction**

40 In the context of high-level radioactive waste (HLRW) geological disposal, large amounts
41 of concrete will be required either for mechanical support for galleries construction in
42 clayey formations or for the sealing of galleries. Evidently, geochemical interactions
43 between concrete and the surrounding clay rock formation and/or the engineered clay
44 barrier will occur.

45 Bentonite will be used in most repository concepts as the engineered barrier surrounding
46 the canister that contains the HLRW. Geochemical interaction between concrete and
47 bentonite will produce smectite dissolution in the clay and incur precipitation of secondary
48 minerals (Savage et al., 2007). There will be also associated effects on the physico-
49 chemical properties of bentonite, like partial pore clogging, decrease of permeability and
50 loss of swelling capacity.

51 Among others, formation of magnesium silicates has been observed in the alkaline reaction
52 zone, at the interface between concrete and clay (Dauzères et al., 2014). This issue became
53 more important when low-pH cementitious materials started to be considered in order to
54 minimize the geochemical interactions with the clay barriers (Calvo et al., 2013; Calvo et
55 al., 2010). High-pH cementitious materials exhibit a low content in Mg, but the addition of
56 supplementary cementitious materials such as fly ash and blast furnace slag in the
57 formulation of low-pH concrete compositions, increase the content of available Al and Mg.

58 Magnesium silicate hydrates (M-S-H) may form in low-pH cement environments by the
59 hydration of MgO at pH 10.5 to produce brucite $[Mg(OH)_2]$, in a first stage, and a
60 subsequent reaction with colloidal silica. The structure of M-S-H phases is not well known
61 since it is described as a low crystalline phase that produce low intensity and broad X-ray
62 diffraction (XRD) reflections (Roosz et al., 2015). However, M-S-H phases have been
63 clearly differentiated from C-S-H phases in chemical structure and occurrence. Silica sheets
64 are present in M-S-H while silica in C-S-H is organized in single chains. Analyses of
65 samples containing both, magnesium and calcium, indicate the formation of separate M-S-
66 H and C-S-H gels, with none or very little uptake of magnesium in C-S-H, or calcium in M-
67 S-H. Therefore, M-S-H and C-S-H do not form solid solutions (Lothenbach et al., 2015). In

agreement with most observations found in nature for the formation of low temperature Mg-rich clay minerals with distinctly Al-free chemical composition, no evidences of Al uptake in M-S-H has been reported in literature regardless the environment in the M-S-H occurrence (e.g. cement-clay interaction, concrete degradation in low-pH concrete formulations). Although possible, very limited occupancy of Al is observed in trioctahedral smectites or Mg in dioctahedral smectites; such substitutions are generally charge-balanced by vacancies. Likewise, Fe^{3+} can substitute Mg within the octahedral sheets of saponite, but complete solid solution between the two end-member compositions is lacking, and there is a chemical gap where true intermediate chemical substitutions are not observed (Michalski et al., 2015).

Nied et al. (2016) studied synthetic M-S-H prepared by mixing MgO and silica fume at different Mg/Si ratios, and cured the samples for 1 year at 20 °C or 3 months at 50 °C. They found Mg/Si ratios in the range 0.7 – 1.5 in M-S-H. Lower ratios are associated with excess of amorphous silica while Mg/Si ratios > 1.3 are associated with presence of brucite. They also predicted talc to act as a precursor at low Mg/Si ratios, and serpentine as a precursor at high ratios.

Mg-enriched zones were observed by the interaction of low-pH concrete with Opalinus Clay associated with carbonates (Jenni et al., 2014), and associated with the decalcification of C-S-H (Dauzères et al., 2016). The Mg-enriched zones present depletion of Ca and reduction of porosity. When high-pH Ordinary Portland Cement (OPC)-type concrete was used, migration of exchangeable Mg from the clay to concrete was observed (Mäder et al., 2017). The latter observation become more evident when FEBEX bentonite is used, due to its high content in exchangeable Mg in the interlayer of smectite (Fernández et al., 2004). Thereby, Fernández et al. (2017) observed large accumulations of Mg at the bentonite side of the interface, precipitating as silicates in various forms (partial transformation of dioctahedral smectite to a tri-octahedral Mg-sheet silicate, but presumably other very similar phases such as M-S-H phases or chrysotile) after 13 years of interaction of a CEM-II-type concrete and FEBEX bentonite in an *in situ* experiment in the Grimsel Test Site (GTS), Switzerland. The accumulation of Mg in the clay side, without reaching the concrete side, must occur due to the low solubility of Mg-phases at high pH when the diffusive alkaline front from the concrete moves towards the bentonite. A mass transfer of Mg from Opalinus Clay able to reach the concrete side was observed by Mäder et al. (2017) when a low-pH concrete-type (ESDRED) was used. In a diffusion experiment of interaction between an alkaline K₂Na-OH solution at pH 13.5 and 90 °C (representative of the aqueous leachate of a OPC-type CEM-I cement) and FEBEX bentonite, Fernández et al. (2013) observed the formation of a non-swelling chlorite-like phase characterized as a brucite monolayer intercalated in the montmorillonite interlayer. Serpentine-like phases were not discarded, although they were not conclusively determined.

In the present study, we combine the study of a long-term laboratory experiment and an *in situ* experiment of interaction between concrete and FEBEX bentonite to focus on three aspects: 1) the geochemical conditions required for the precipitation of Mg-silicates phases in the alteration zone at the interface (i.e. chemical compositions of concrete and bentonite and their interaction processes); 2) the structural identification of the Mg-silicates, and 3) the implications of the occurrence of these mineral phases for the disposal of HLRW.

Materials and Methods

FEBEX bentonite, original from Almería, Spain (Caballero et al., 2005), was used in a compacted form in laboratory and *in situ* experiments. The FEBEX bentonite is characterized by a high content in smectite that exhibits a high content in exchangeable Mg (Huertas et al., 2001) with respect to many other well-known bentonites.

High-pH CEM-I and CEM-II-type concretes have been used in the laboratory and *in situ* experiments, respectively.

The samples examined in the present study have been carefully taken from the alkaline alteration zone formed at the interface between concrete and bentonite. These samples were selected either from the HB6 laboratory experiment (sample labelled as *lab 10 a, CEM-I HB6*) or the *in situ* experiment performed in the FEBEX gallery at the GTS, Switzerland (samples labelled as *in situ* CEM-II, reference location). Three samples have been indistinctly used to describe the results of the *in situ* experiment. Their reference location in the gallery are 32-4, 35-3 and 34-10. The nomenclature can be consulted in Fernández et al. (2017), however the 3-dimensions position of the samples in the gallery is not relevant for the purpose of the present study.

It is considered convenient, for the identification of the mineralogical transformations, to make use of two additional samples that may serve as reference for comparison with the samples studied in the present work: a Mg-FEBEX bentonite and an altered Mg-FEBEX bentonite. The Mg-FEBEX bentonite was used in previous studies (Fernández et al., 2009) and consists of a pre-treated natural FEBEX bentonite washed with a MgCl_2 solution to replace all exchangeable cations in the interlayer of smectite by Mg. Then, the sample is washed with ethanol in a first stage and water in a second stage until the measurement of the electrical conductivity indicates that the excess of salts is washed out. Also, when pertinent, we have introduced additional samples from other previous studies that show optimal results for comparison with the experiments presented in this study. The description of these reference samples is given accordingly to the comparison of results. The altered Mg-FEBEX bentonite was obtained by alkaline interaction through a diffusion experiment with a K,Na-OH solution at pH 13.5. The experiment was run for 1.5 years at a constant temperature of 90 °C (Fernández et al., 2010).

The HB laboratory experiments were designed by a cylindral column containing a FEBEX bentonite compacted at 1.65 g/cm^3 (dry density) and a high-pH concrete with a composition based on a sulforesistant OPC CEM-I 42.5 R/SR cement type without mineral additions, inserted in a Teflon sleeve of 70 mm inner diameter (Alvarez et al., 2008). The concrete block had a length of 30 mm and the bentonite block of 71.5 mm. The cells were heated at 100 °C from the bottom (bentonite side) and, simultaneously, hydrated with a synthetic saline solution representative of a Spanish clayey formation from the concrete side. The solution is dominated by Na^+ ($1.3\text{e-}1 \text{ M}$), Ca^{2+} ($1.1\text{e-}2 \text{ M}$), Mg^{2+} ($8.2\text{e-}2 \text{ M}$), SO_4^{2-} ($7.0\text{e-}2 \text{ M}$), Cl^- ($2.3\text{e-}2 \text{ M}$) and HCO_3^- ($1.8\text{e-}3 \text{ M}$) and exhibits pH 7.54 and a $\log P(\text{CO}_2) = -2.65$ (Turrero et al., 2006). These conditions simulated the heat emitted by the radioactive decay of the spent fuel contained in the canister and the hydration to the engineered barriers system from the host clay formation, respectively. The HB experiments were run under the

described set up at different time spans from 6 months to 10 years. The samples examined in the present study correspond to the experiment performed for 10 years (HB6). A parallel experiment performed under the same experimental conditions but dismantled after 4.5 years (HB4) produced precipitation of brucite and aragonite at the upper concrete side in contact with the hydration source. Therefore, Ca, Mg and carbonates were assumed to be retained at the upper side of the concrete disc, opposite to the bentonite interface (Cuevas et al., 2012).

The *in situ* FEBEX experiment performed at the GTS underground research laboratory was dismantled after 18 years of operation, but interface samples between the bentonite and the concrete plug, that was constructed in a second operational phase, were studied after 13 years of interaction. The concrete plug was composed of a CEM-II A-L 35.5 R cement with additions of nanosilica, polypropylene and steel fibres. The FEBEX bentonite was inserted in blocks compacted at a dry density of 1.7 g/cm^3 . The engineered barrier system was hydrated in the gallery with a low electrical conductivity porewater caused by the few transmissive fractures in the granitic host rock. A more detailed description of the experiment can be found elsewhere (Alonso et al., 2017; Fernández et al., 2017).

Only small amounts of samples were required for the analytical procedures used in the present study. These samples were scraped away from well preserved concrete-bentonite interfaces and stored in closed vials to prevent further hydration in contact with atmosphere.

The characterization of the solid phase was performed by a set of analytical techniques.

An X-PERT Panalytical diffractometer with an X-CELERATOR X-ray detector (XRD) was used for the mineralogical identification. The XRD patterns registered on bulk randomly oriented dried powder samples were recorded in an angular range of $3\text{--}70^\circ 2\theta$, using Cu K α 1 radiation ($\lambda = 1.54056 \text{ \AA}$) and a Ge monochromator with divergence and reception slits of 2 and 0.6 mm, respectively. The diffractometer operated at a voltage of 40 kV and an intensity of 40 mA.

An INCAx-sight Oxford Instruments® Energy Dispersive X-ray analyser coupled to a Hitachi S-3000N Scanning Electron Microscope (SEM-EDX) was used for the identification of morphologies and analyses of chemical compositions. The measurement parameters used for the measurement were: livetime = 40 s, acceleration voltage = 20 kV, range of probe current = 70–120 mA. The EDX quantification was performed by means of internal standard quantitative analyses.

Thermogravimetric Analysis (TGA) was performed by a Differential Scanning Calorimetry (DSC)/Differential Thermal Analysis (DTA)/TGA Q600 TA Instruments® module from 25 to 1000 °C with a temperature increment rate of 10 °C/min under a nitrogen gas flow. Only 0.1 g of bulk samples ground to $< 5 \text{ }\mu\text{m}$ were required for these analyses.

Fourier transform infrared spectrometry (FTIR) spectra of the samples were obtained using a Nicolet 6700 FTIR spectrometer in transmission mode with a deuterated triglycine sulfate (DTGS) KBr detector and recording over the middle-IR region spectral range ($4000\text{--}400 \text{ cm}^{-1}$) with a resolution of 2 cm^{-1} in an atmosphere continuously purged from water and

atmospheric CO₂. For these analyses, 2 mg of bentonite was grinded in a Retsch RM200 mortar grinder with a pestle of agate and mixed with 100 mg of KBr.

Solid-state Cross-Polarization Magic Angle Spinning ²⁹Si and ²⁷Al Nuclear Magnetic Resonance (CP/MAS-NMR) spectra were acquired using a Bruker AV-400-WB spectrometer equipped with a 4 mm MAS-NMR probe, with the samples spinning at a rate of approximately 10 kHz. The operating frequency was 79.49 MHz, using 60 s excitation pulses ($\pi/2$) at 50 kHz. The chemical shifts of ²⁹Si resonances were evaluated in relation to kaolinite (-91.5 ppm) and tetramethylsilane (TMS) as secondary and primary references, respectively. The ²⁷Al frequencies were referenced externally to a 0.1 M AlCl₃ solution ($\delta = 0$ ppm).

Results

X-ray diffraction

The XRD powder pattern of the altered Mg-FEBEX sample is characterized by a non-expandable 14.1 Å basal spacing (001 reflection) with an asymmetric tail towards higher angles that ends in a 7.4 Å reflection (002), interpreted (with the aid of HR-TEM) as a brucite intercalation in the smectite interlayer forming a chlorite-like structure that conserves the dioctahedral character (Fernández et al., 2013). All the presented patterns, except the one of the Mg-FEBEX bentonite sample show a broad step related to the reflection at 7.4 Å (Fig. 1).

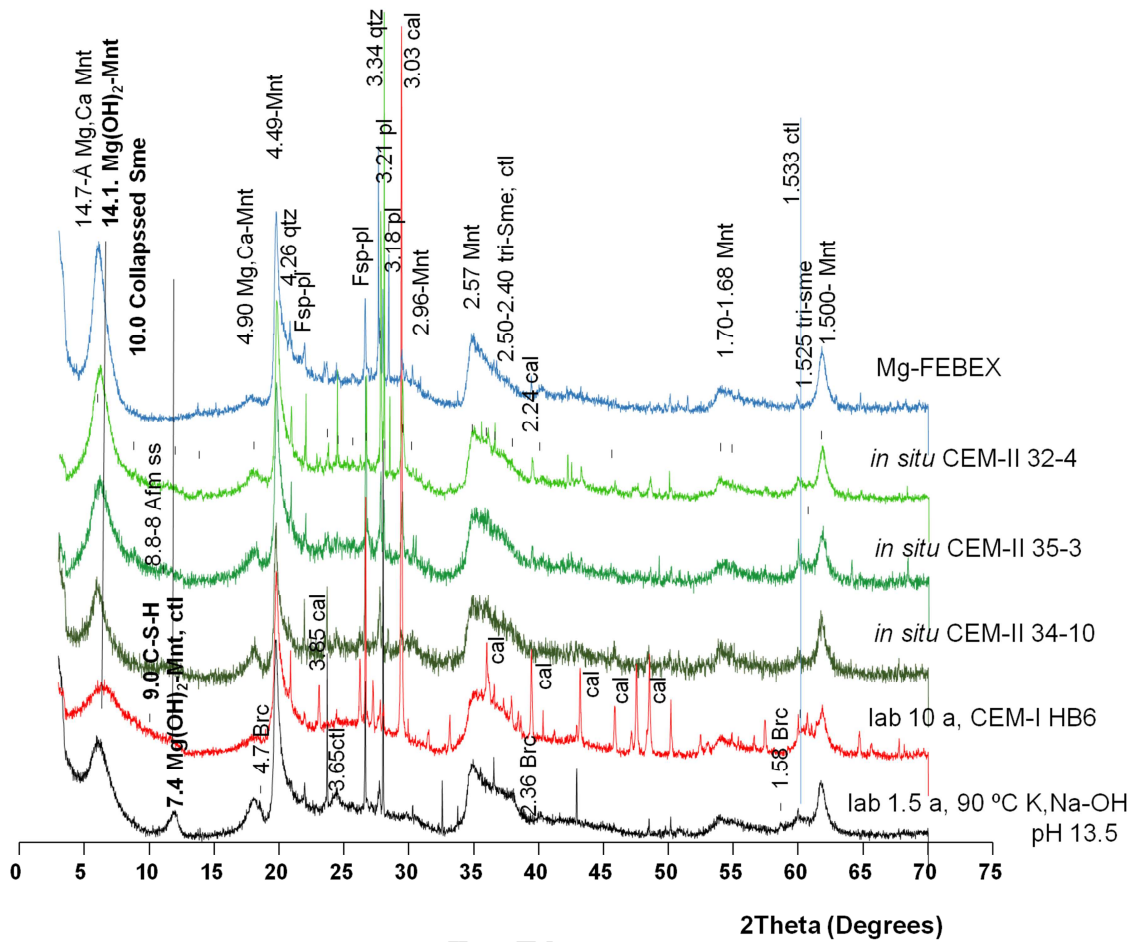


Fig 1: XRD on randomly oriented powder patterns of bentonite samples at the alkaline alteration zone. Black: reference altered Mg-FEBEX bentonite sample; Red: lab 10 a, CEM-I HB6 sample; Green: in situ CEM-II samples; Blue: reference Mg-FEBEX bentonite sample. Mnt = montmorillonite; Sme = smectite; C-S-H = calcium silicate hydrates; ctl = chrysotile; qtz = quartz; Fsp-pl = feldspar-plagioclase; cal = calcite; Brc = brucite.

Brucite is only clearly detected in the reference altered Mg-FEBEX bentonite sample by the reflection at 4.78 Å (Fig. 2a), but some traces are also observed in the samples of the lab 10 a, CEM-I-HB6 experiment and the *in situ* experiments.

The region at 35-40 °2θ shows a decreasing regular slope in the Mg-FEBEX sample. In the other samples, there is a visible hump, centred at 36-37 °2θ, characteristic of serpentine and/or trioctahedral sheet silicate minerals. This is further confirmed by the presence of the 1.53-1.52 Å (060) reflection. A detail of this reflection (Fig. 2b) shows the predominance of the 1.533 Å in the *in situ* samples, characteristic of a 1:1 phyllosilicate serpentine, while in the lab 10 a, CEM-I-HB6 sample, the reflection is observed at 1.525 Å, more typical of a 2:1 trioctahedral smectite or talc-like mineral.

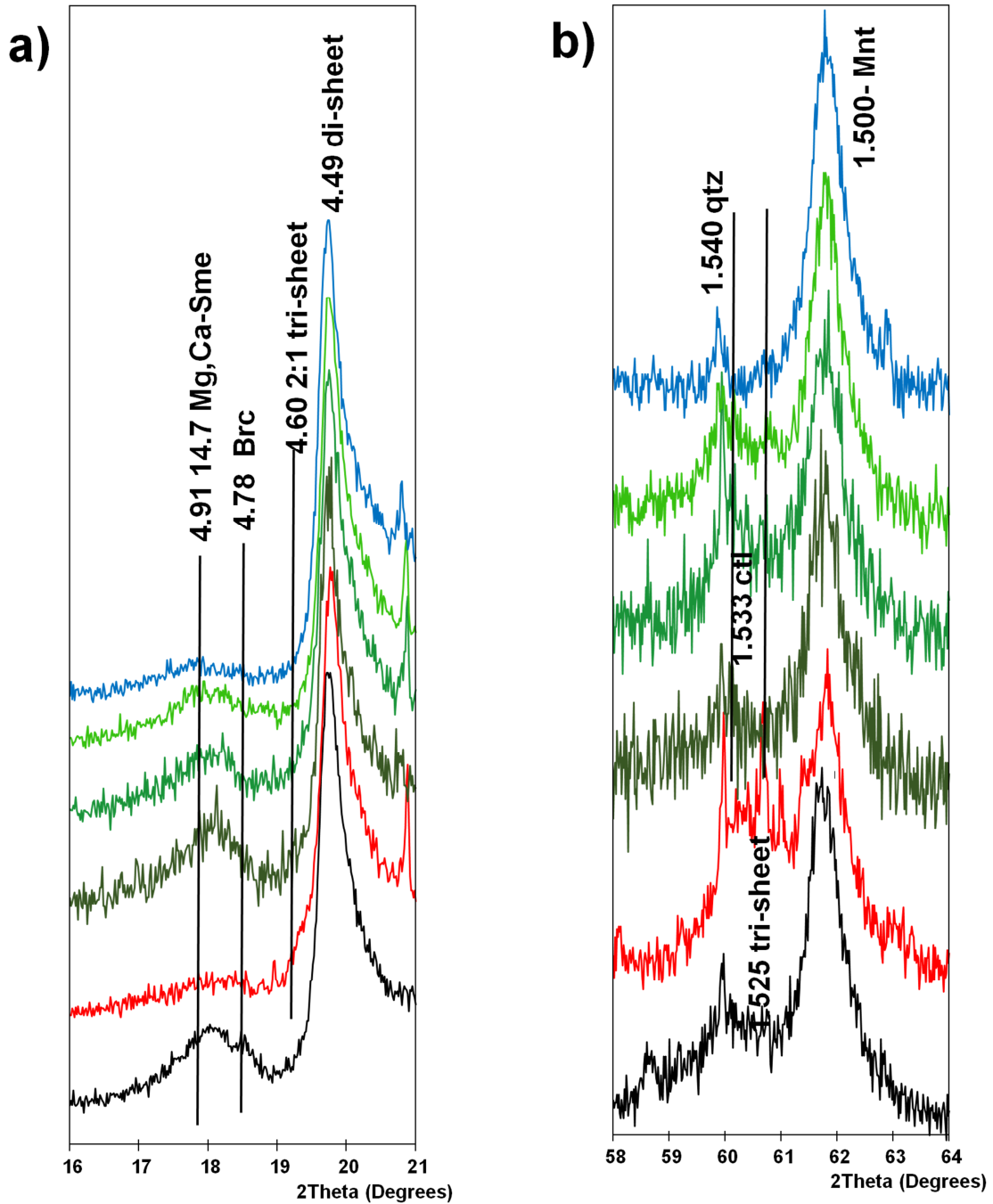


Fig 2: Detail of XRD reflections of samples shown in Fig. 1, in the range of a) 16-21 °2θ where the reflection characteristic of brucite (4.78 Å) is identified, and b) 58-64 °2θ where the d(060) is displaced to 1.533 Å in the samples of the in situ experiment (green), and to 1.525 Å in the sample of the laboratory experiment (red). Di-sheet, tri-sheet = dioctahedral or trioctahedral sheet silicate.

Thermogravimetric analysis

Brucite or M-S-H are normally detected in the range of temperatures 450-500 °C. A comparison of the reference and altered samples is shown in Fig. 3 to evidence the alteration effects. The original FEBEX bentonite sample presents a characteristic peak in the first derivative of the TG curve (DTG) at 610 °C, caused by dehydroxylation in the smectite. An additional peak at 465 °C is observed in a FEBEX bentonite sample treated with MgCl and a K,NaOH solution (FEBEX-brucite sample in Fig. 3). In these conditions, formation of brucite was evidenced, and confirmed by DTG. In the samples from the lab 10 a, CEM-I-HB6 and *in situ* experiments the DTG show higher temperatures that would agree with brucite dehydroxylation from the interlayer of smectite. 660 °C is near the temperature of dehydroxylation of serpentine, being the range 500-660 °C the temperatures where montmorillonite and serpentine can overlap their dehydroxylation effects. In the lab 10 a, CEM-I-HB6 experiment, however, the presence of calcite, detected by the peak observed at 706 °C, does not allow to better discriminate the dehydroxylation effects.

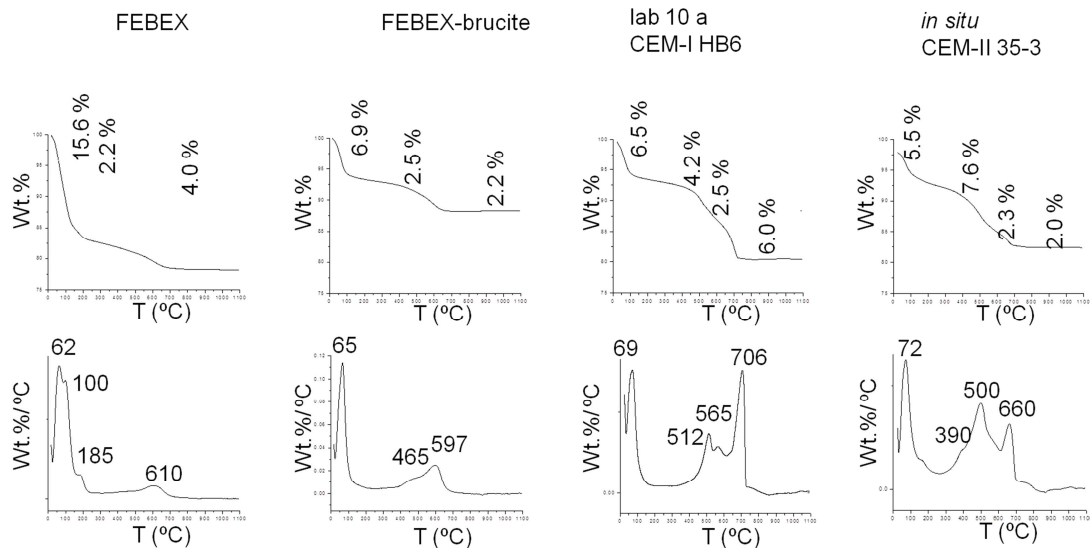


Fig 3: Thermogravimetric (upper figures) and differential thermogravimetric (lower figures) curves for FEBEX bentonite, a treated FEBEX bentonite with presence of brucite, the lab 10 a, CEM-I-HB6 experiment and the *in situ* CEM-II 35-3 sample, from left to right.

Scanning Electron Microscope

An extensive inspection of small samples selected from the alkaline alteration zone in bentonite was performed by SEM-EDX. Several lamellar morphologies, such as those presented in Figs. 4 and 5, are observed in the bentonite altered zone in the laboratory and the *in situ* experiments. A large number of EDX measurements on the surface of these morphologies provides an averaged Mg/Si ratio close to 0.7. The range of the Mg/Si ratio may vary between 0.58 and 0.75 (based on 20 analyses), but it might be considered that

regions close to the spots analyzed have some influence on the compositions obtained and the complex mineralogy presented in these zones with coexisting minerals of different composition produces some disturbances in the chemical analyses. Although C-(A)-S-H phases and carbonates coexist in this region with magnesium silicates, it is remarkable the absence of Ca in the chemical composition of the lamellar morphologies, in agreement with the chemical differentiation observed by (Lothenbach et al., 2015) for the Ca and Mg silicate hydrates.

The altered sample from the bentonite side of the lab 10 a, CEM-I-HB6 experiment is characterized by hardened clay surfaces with abundant presence of lamellar morphologies, as observed by SEM in Fig. 4a. EDX analyses performed on clean surfaces of the lamellar morphologies, with low contamination of the surrounding clayey matrix, show Mg/Si ratios near 0.7 and negligible content of Ca. In addition, other morphologies have been identified at point locations, such as prismatic forms of ettringite, columnar morphologies (Fig.4b) identified as brucite, mixed with altered Mg silicates that provide EDX compositions with Mg/Si ratios in the range 1.2-1.3, and the flake-like morphologies of calcium carbonate shown in Fig. 4c.

The SEM technique is inconclusive for discriminating among calcium carbonate polymorphs because the morphology of each calcium carbonate polymorph is not unique (Ni and Ratner, 2008). However, Chakrabarty and Mahapatra (1999) observed a change from the typical needle-like morphology of aragonite to a flake-like shape under certain crystallization conditions. Aragonite was previously observed at the concrete-bentonite interface in previous HB experiments of shorter duration (Turrero et al., 2011).

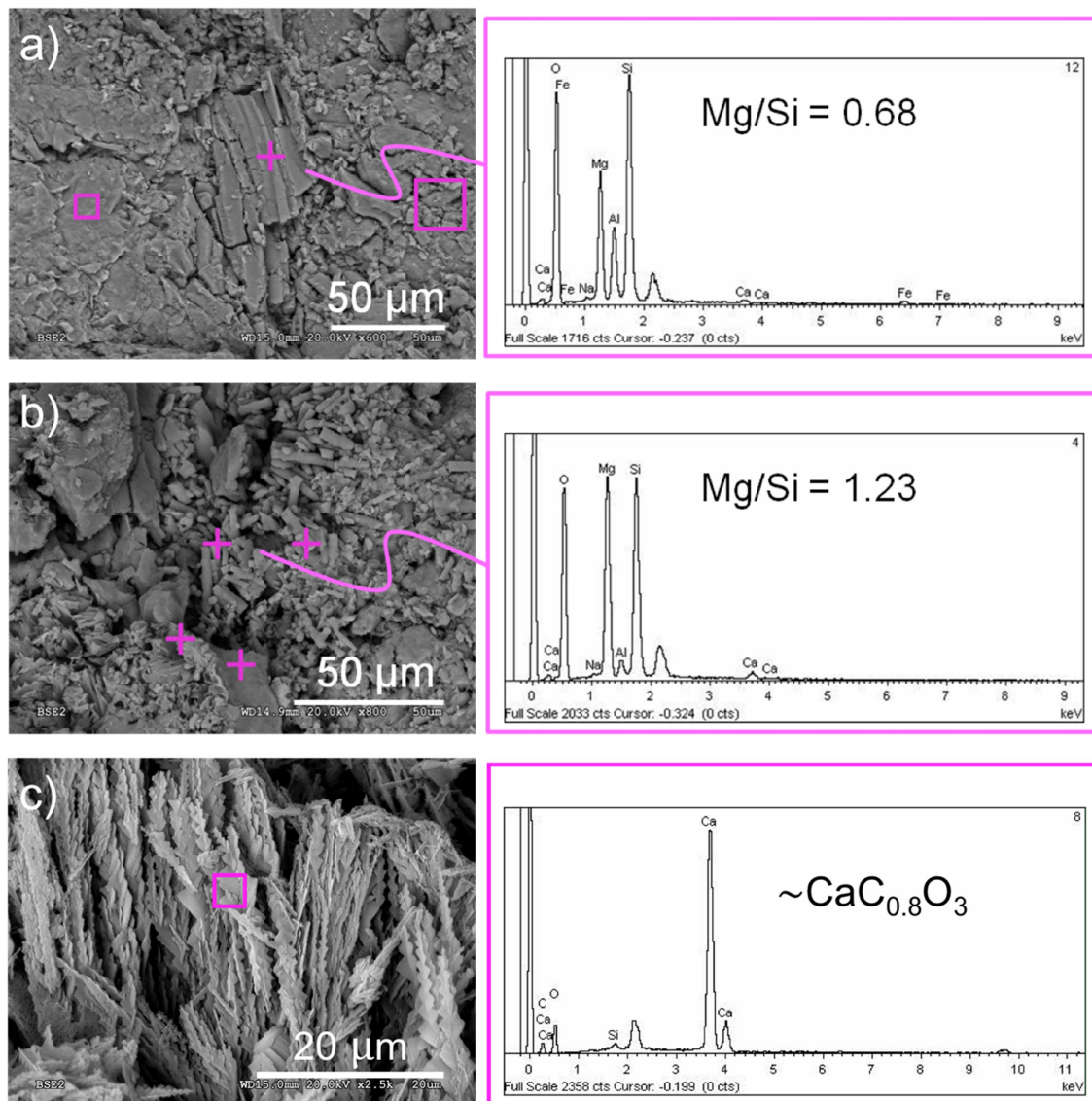


Fig 4: SEM images obtained from the lab 10 a, CEM-I-HB6 experiment. a) formation of a Mg-silicate with lamellar morphology within a clayey matrix; b) Mg-silicate with columnar morphology, and c) flake-like morphologies of calcium carbonate. EDX analyses are provided on the selected spots.

Lamellar morphologies were also observed in the *in situ* experiment. Several EDX analyses performed on the surface of these morphologies revealed Mg/Si ratios close to 0.7 as shown in Figs. 5 a) and b) for the CEM-II 34-10 sample. No other structures were observed by SEM in the *in situ* samples other than these lamellar morphologies and the shapeless clay matrix.

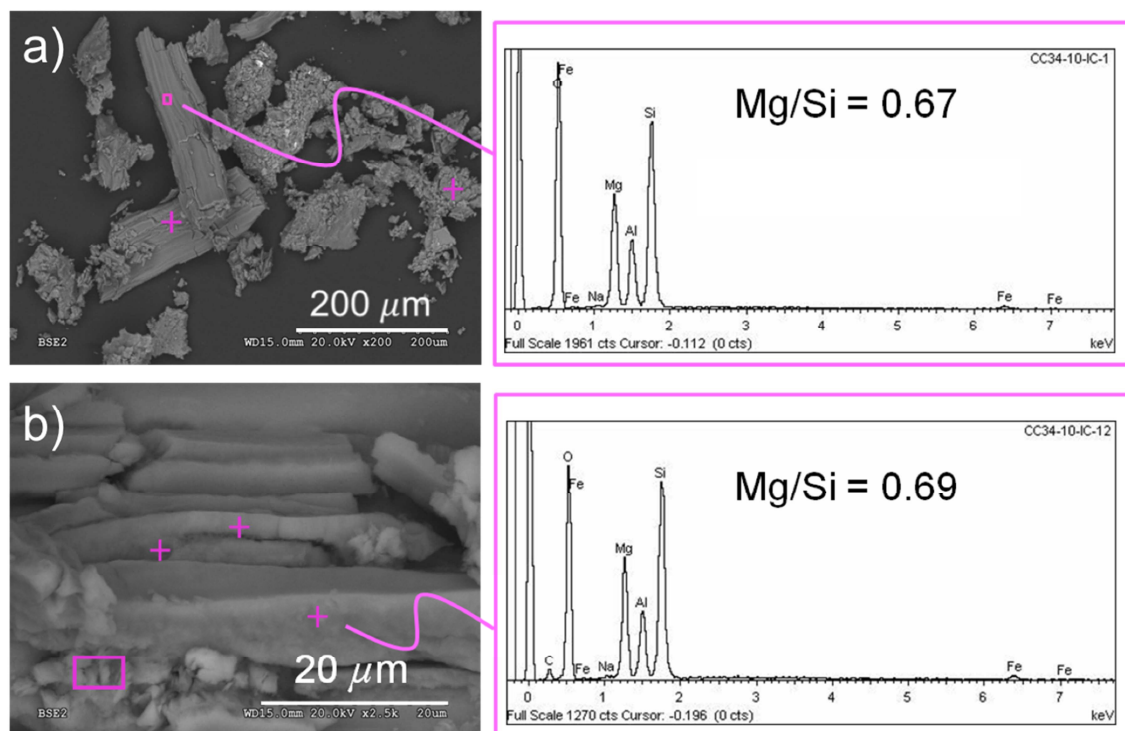


Fig 5: SEM images obtained from the *in situ* CEM-II 34-10 sample. a) Mg-silicate with lamellar morphology; b) detail of the Mg-silicate with lamellar morphology at higher magnification. EDX analyses are provided on the selected spots.

Infrared spectroscopy

IR spectra of samples lab 10 a, CEM-I-HB6 and *in situ* CEM-II 35-3 are presented in Fig. 6 against the reference FEBEX montmorillonite (fraction $< 2 \mu\text{m}$ of the FEBEX bentonite). The absorption band at 3624 cm^{-1} , typical of smectites with high content of Al in octahedral sites (Madejová and Komadel, 2001) is observed in all of the samples (Fig. 6). However, the band at 3708 cm^{-1} , attributed to trioctahedral 2:1 sheet silicates, where all octahedral positions are filled with Mg, is only observed in the altered samples indicating partial transformation of the original smectite structure. Bending vibrations of hydroxyl groups associated with Al and Mg cations, i.e., 906 cm^{-1} (Al-Al-OH) and 839 cm^{-1} (Al-Mg-OH) confirm the substitution in the octahedral sheets (Tyagi et al., 2006). Absorption bands of carbonates (at 1800 , 1430 , 875 and 710 cm^{-1}) are also visible in the altered samples but not present in the reference sample. The broad bands at 3421 and 1646 cm^{-1} correspond to the stretching and bending vibrations of the hydroxyl groups of water molecules present in the clays and the bands at 1114 and 1039 cm^{-1} , also observed in the three samples, are assigned to Si-O stretching out-of-plane and in-plane, respectively.

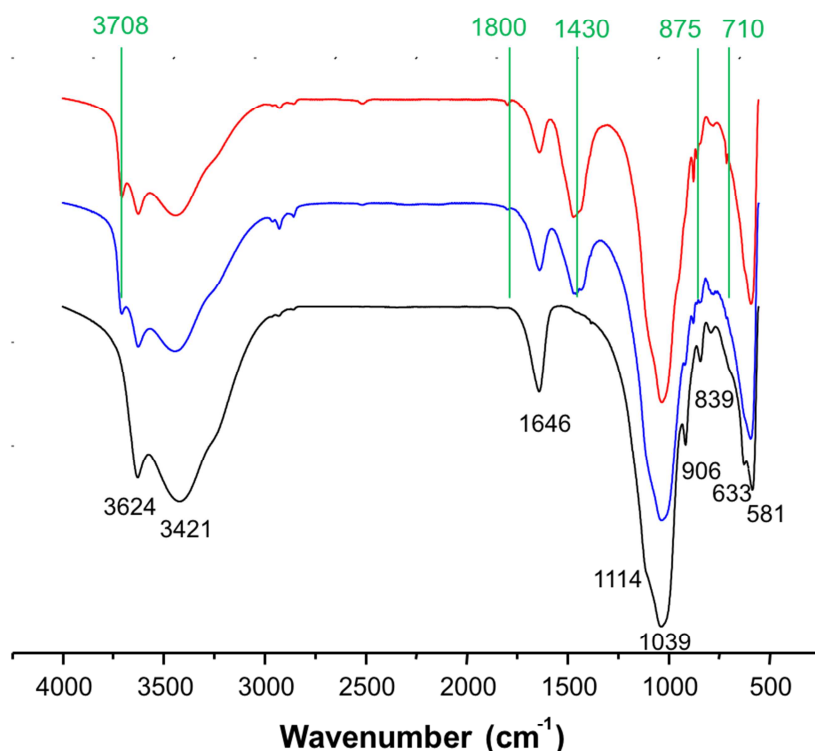


Fig 6: Infrared spectra of samples lab 10 a, CEM-I-HB6 (upper, red), in situ CEM-II-35-3 (medium, blue) and reference FEBEX < 2 μm (lower, black).

Nuclear Magnetic Resonance

The main signal of the ^{29}Si NMR spectrum in montmorillonite ($\delta = -94$ ppm) is attributed to $^{\text{IV}}\text{Si}$ (Q^3) hosted in tetrahedral sites, bonded to other 3 silicon atoms in the structure (Fig 7). This signal, observed in the three compared samples, exhibit a broader resonance for the *in situ* CEM-II 35-3 sample and indicates larger local disordering of the Si environment. The ^{29}Si chemical shifts observed in the *in situ* CEM-II 35-3 sample at -86 and -83 ppm are attributed to Q^2 [0Al] and Q^2 [1Al] while the chemical shift at -85 ppm observed in the lab 10 a, CEM-I-HB6 sample is attributed to Q^2 [0Al]. These same signals were previously observed in an alkaline alteration batch experiment of FEBEX montmorillonite and were assigned to the formation of C-S-H (Q^2 [0Al]) and C-A-S-H (Q^2 [1Al]) phases (Fernández et al., 2016). In addition, chemical shifts at -112, -103 and -90 ppm (Q^2 , Q^3 and Q^4 , respectively) observed in the *in situ* sample could be attributed to chrysotile (Wypych et al., 2005), although the resonance is that low that signals are not conclusive. Shoulders observed at -97 and -99 ppm have not been assigned, although (Weiss et al., 1987) reported a $\delta = -98.5$ ppm corresponding to a trioctahedral Q^3 [0Al] for a crystalline talc.

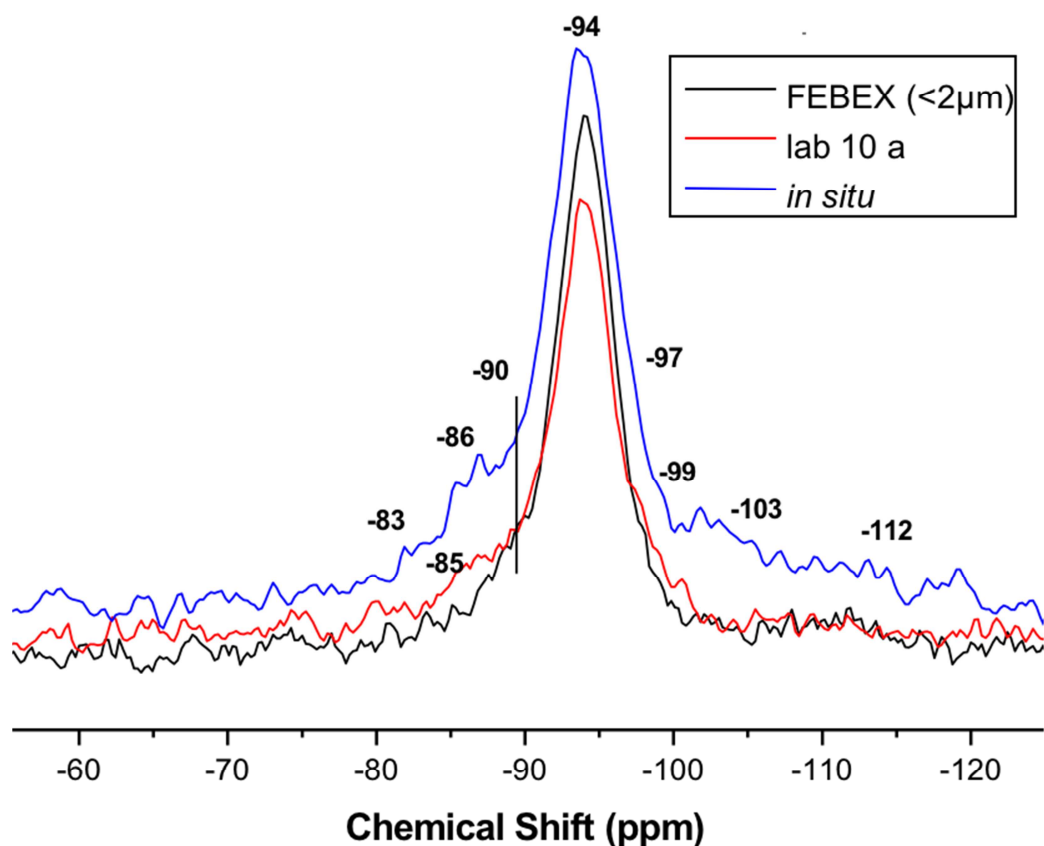


Fig 7: ^{29}Si NMR spectra of samples lab 10 a, CEM-I-HB6 (red), in situ CEM-II-35-3 (blue) and reference FEBEX $< 2 \mu\text{m}$ (black).

A decrease in the intensity of the octahedral $^{\text{VI}}\text{Al}$ (3 and 9 ppm) is observed by ^{27}Al NMR in the altered samples with respect to the reference sample, while the tetrahedral $^{\text{IV}}\text{Al}$ suffers a shift from -68 to -57 ppm that could be in agreement with the formation of C-A-S-H phases according to (Komarneni et al., 1987), who reported a resonance at -59 ppm attributed to an impurity of Al in tetrahedral coordination during the characterization of a synthetic jennite (Fig. 8).

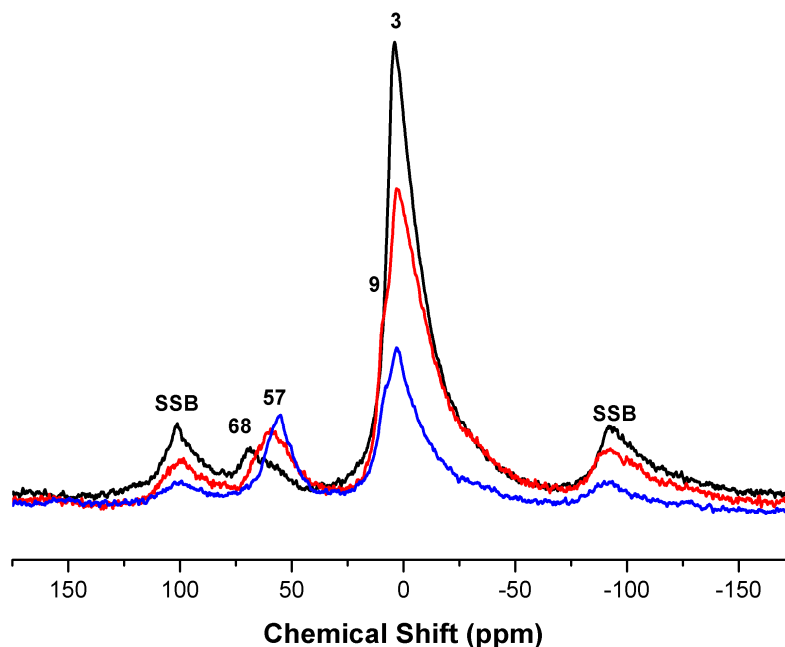


Fig 8: ^{27}Al NMR spectra of samples lab 10 a, CEM-I-HB6 (red), in situ CEM-II-35-3 (blue) and reference FEBEX $< 2\ \mu\text{m}$ (black). SSB = Spinning Side Bands.

Discussion

In order to establish a basis for discussion on the nature of the Mg phases formed in bentonite near the concrete-bentonite interface, typical atom ratios of structural cations in different minerals have been calculated. They are compared with atom ratios measured by SEM-EDX on dry polished sections at the bentonite side of the interface, prepared to produce elemental maps. The lab 1.5 a, 90 °C K,Na-OH alkaline experiment is compared with the *in situ* CEM-II 34-10 experiment in Fig. 9.

A theoretical composition of a FEBEX montmorillonite-brucite with chemical formula $\text{Mg}_3(\text{OH})_{5.5}\text{Al}_{1.5}\text{Mg}_{0.5}\text{Si}_4\text{O}_{10}(\text{OH})_2$ has been used to calculate the Mg/Si atom ratio = 0.87 used in Fig. 9, to plot line 1. In the same way, the chemical composition $\text{Ca}_{0.125}\text{Mg}_{2.75}\text{Si}_4\text{O}_{10}(\text{OH})_2$ has been used to plot line 2 (Mg/Si ratio = 0.69) as a reference for a trioctahedral smectite. An ideal FEBEX montmorillonite would exhibit a constant Al/Si atom ratio = 0.375 for a chemical composition $\text{Ca}_{0.25}\text{Al}_{1.5}\text{Mg}_{0.5}\text{Si}_4\text{O}_{10}(\text{OH})_2$. Line 3 in Fig. 9 simply reproduces the Al/Si ratio observed in bentonite far from the alkaline interface where negligible structural alteration was detected. The same reference Al/Si is observed in both samples around 0.34 (lower than the calculated 0.375 for montmorillonite) because it includes all the accessory minerals present in bentonite, increasing the amount of Si. Line 4 (red) in Fig. 9 reproduces the reference value of the original bentonite for a theoretical ratio

between exchangeable and structural cations. The experimental ratio has been calculated considering the sum of Na, K and Ca atoms, divided by the sum of Al, Mg and Fe atoms, excluding Si ($\frac{Na+K+Ca}{Al+Mg+Fe}$). This ratio is considered as an indicator of structural transformation of montmorillonite. Finally, line 5 in Fig. 9 reproduces the Mg/Si ratio (around 0.12) observed in the non-altered bentonite far from the alkaline interface.

The alteration thickness observed in both compared samples reach 4 mm in the lab 1.5 a, 90 °C K,Na-OH sample and 2 mm, with a more visible alteration in the first 0.5 mm, in the *in situ* CEM-II 34-10 sample. In this region, the Mg/Si ratio is compatible with the intercalation of a brucite layer within the smectite interlayer and with the formation of a trioctahedral smectite, although in the case of the *in situ* sample even an excess of Mg is observed.

The Al/Si ratio is maintained constant and approximately equal to the original montmorillonite in Mg-bentonite K,Na-OH altered sample. This is consistent with the presence of brucite interlayers and with the remaining dioctahedral sheet silicate frame.

In order to explain the trioctahedral effect the calculation of the ratio between the potential exchangeable cations and structural cations (line 4) is used. Near to the concrete interface, the M_{exc}/M_{str} ratio increases in the *in situ* sample due to the high content in Ca attributed to carbonates instead of exchangeable Ca, but then this ratio decreases below the reference level as observed in the lab 1.5 a, 90 °C K,Na-OH experiment. The M_{exc}/M_{str} minimum does not correspond with the experimental Mg/Si maximum perhaps because Mg is partly exchangeable and could have some contribution, especially far from the interface. Intercalation of brucite in the interlayer of smectite may still allow presence of exchangeable cations in order to compensate layer charge, therefore, a slight decrease is compatible with the precipitation of serpentine-like minerals or talc. If some talc or serpentine precipitate in significant amounts, the Al/Si ratio should decrease according to its chemical compositions, since there is no Al in these mineral phases.

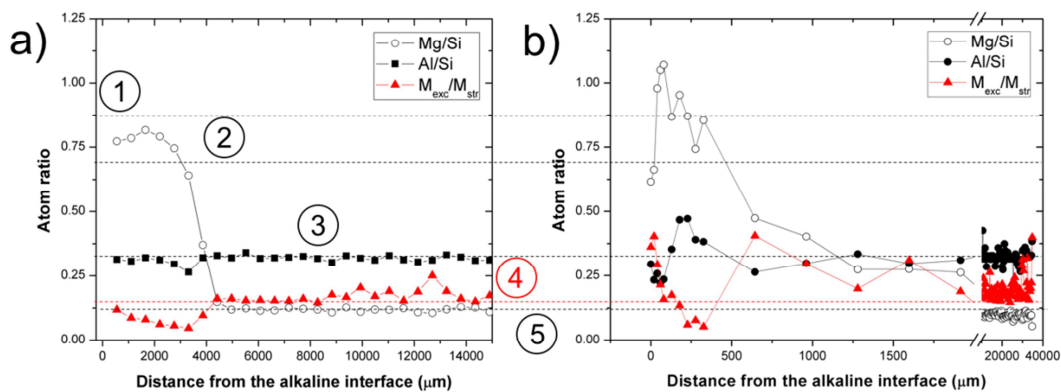


Fig 9: Atom ratios in bentonite samples as a function of the distance to the alkaline interface in a) the lab 1.5 a, 90 °C K,Na-OH reference experiment (Fernández et al.,

2013) and b) the in situ CEM-II 34-10 sample. Dashed lines indicate: (1) Mg/Si atom ratio = 0.87 characteristic of FEBEX montmorillonite - brucite phase, (2) Mg/Si atom ratio = 0.69 for a trioctahedral smectite, (3) reference Al/Si atom ratio of FEBEX bentonite, (4) reference M_{exc}/M_{str} ratio of FEBEX bentonite (in red) and (5) reference Mg/Si atom ratio of FEBEX bentonite.

The formation of Mg silicate phases in the bentonite barrier near the concrete may have some consequences in terms of geochemical reactivity. Cuevas et al. (2016) performed a series of experiments in small cells using a lime mortar in contact with either a common FEBEX bentonite or a pretreated “aged” FEBEX bentonite depleted in exchangeable Mg and enriched in K. The cells were hydrated with a synthetic clay water (Na^+ , Ca^{2+} , SO_4^{2-} saline solution). The experiments were run at 60 °C for 18 months. Results by SEM-EDX revealed that precipitation of Mg silicates that formed in the experiment run with the common FEBEX bentonite had capacity to buffer the alkaline front of the lime mortar.

Fig. 10 compares the results obtained by Cuevas et al. (2016) in both types of cells. An increase of Mg can be observed in bentonite near the interface (Fig. 10b) in agreement with the formation of Mg silicate phases. Some depletion of Ca is observed at the mortar side. The excess of Ca precipitates at the interface, in the bentonite side, but only over the first mm of thickness, just before the maximum of Mg. The alteration in bentonite is associated with a decrease of porosity. When Mg silicates do not form, as observed in the case with the bentonite depleted in exchangeable Mg (Fig. 10a), the excess of Ca advances towards the bentonite in larger extension and the decrease of porosity is not that evident.

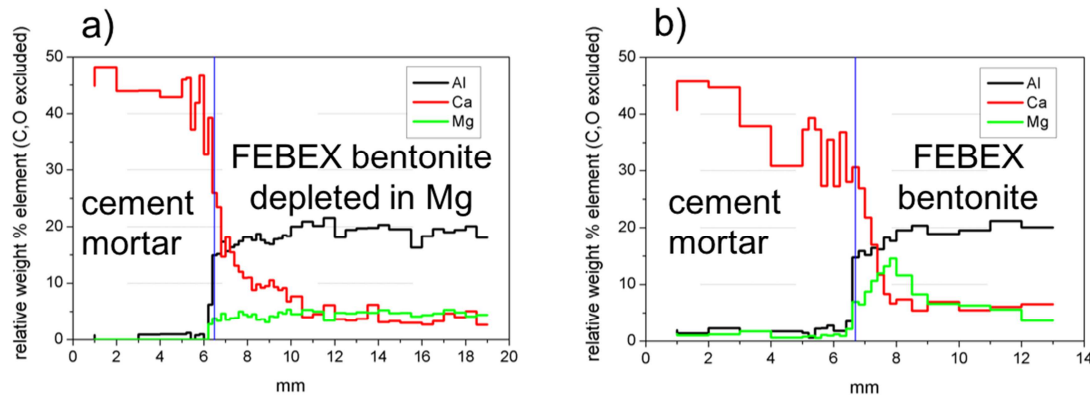


Fig 10: Relative weight % of Al (black), Ca (red) and Mg (green) as a function of distance in lime mortar-bentonite cells in: a) experiment with bentonite depleted in exchangeable Mg; b) experiment with natural bentonite. The interface is indicated by a perpendicular blue line. Results are taken from (Cuevas et al., 2016).

Therefore, it might be considered that precipitation of Mg silicate phases has positive effects on the bentonite barrier performance to reduce the porosity and buffer the Ca alkaline front. Brucite intercalation in the smectite interlayer, rather than M-S-H

precipitation, produces a reversible alteration of smectite, maintaining the barrier properties of bentonite. However, it has to be considered that results presented in the present study are based on the interpretation of multiple sample analyses and are not easily observable in every sample even when the used bentonite, FEBEX, has a high content in exchangeable Mg, not present in many other bentonites studied for their use as barrier for radioactive waste confinement. Therefore, the impact of the precipitation of Mg phases on other bentonite, such as the MX-80, could be lower.

Conclusions

Formation of Mg-silicates is systematically observed in the clay side of the alkaline interaction zone between concrete and FEBEX bentonite. The identification of the Mg-silicates is not trivial but, in addition to a chlorite-like phase (brucite intercalated in a 2:1 montmorillonite structure), either 1:1 serpentine-type (in *in situ* experiments) or 2:1 trioctahedral phyllosilicates (in the lab 10 a, CEM-I-HB6 experiment) have been observed rather than M-S-H phases, typically observed in concrete. The Mg/Si atom ratios are in the range 0.7 – 1.3, like that in M-S-H found previously in synthesis experiments or in concrete pores facing clay materials. Al is still present in the structure and virtually conserves its proportions to Si in the mixed structures. Then, brucite intercalation may be initially the predominant reaction. Further ageing process will drive to the development of the mineral assemblage including di- and trioctahedral sheet silicates. The formation of Mg-silicates in the alkaline reaction zone inhibits the alkaline Ca front arising from concrete. The present study confirms a possible upscaling from laboratory experiments to the repository scale due to the similar alteration observed in both experiments.

Acknowledgements

The results presented in this manuscript contains partly work of the FEBEX-DP project that was financially supported by the FEBEX-DP consortium (www.grimsel.com/gts-phase-vi/febex-dp). Authors thanks the revision performed by two anonymous reviewers and the Associate Editor, Adrian Bath.

References

- Alonso, M.C., Calvo, J.L.G., Cuevas, J., Turrero, M.J., Fernández, R., Torres, E., Ruiz, A.I., 2017. Interaction processes at the concrete-bentonite interface after 13 years of FEBEX-Plug operation. Part I: Concrete alteration. *Physics and Chemistry of the Earth Parts A/B/C* 99, 38–48. doi:10.1016/j.pce.2017.03.008
- Alvarez, E.T., Escribano, A., Turrero, M.J., Martín, P.L., Peña, J., Villar, M.V., 2008. Temporal Evolution of the Concrete-Bentonite System under Repository Conditions, in: *Materials Research Society Symposium Proceedings*. Materials Research Society. doi:10.1557/proc-1124-q07-09

480 Caballero, E., de Cisneros, C.J., Huertas, F.J., Huertas, F., Pozzuoli, A., Linares, J., 2005.
 481 Bentonites from Cabo de Gata Almería, Spain: a mineralogical and geochemical overview.
 482 Clay Minerals 40, 463–480. doi:10.1180/0009855054040184

483 Calvo, J.L.G., Alonso, M.C., Hidalgo, A., Luco, L.F., Flor-Laguna, V., 2013. Development
 484 of low-pH cementitious materials based on CAC for HLW repositories: Long-term
 485 hydration and resistance against groundwater aggression. Cement and Concrete Research
 486 51, 67–77. doi:10.1016/j.cemconres.2013.04.008

487 Calvo, J.L.G., Hidalgo, A., Alonso, C., Luco, L.F., 2010. Development of low-pH
 488 cementitious materials for HLRW repositories. Cement and Concrete Research 40, 1290–
 489 1297. doi:10.1016/j.cemconres.2009.11.008

490 Chakrabarty, D., Mahapatra, S., 1999. Aragonite crystals with unconventional
 491 morphologies. Journal of Materials Chemistry 9, 2953–2957. doi:10.1039/a905407c

492 Cuevas, J., Fernández, R., Ruiz, A.I., de Soto, I.S., Vigil de la Villa, R., Escribano, A.,
 493 Torres, E., Villar, M.V., Turrero, M.J., 2012. Mineral reaction front developed in a 4.5
 494 years test for the study of concrete-bentonite interface. Macla 16, 128-129.

495 Cuevas, J., Ruiz, A.I., Fernández, R., Torres, E., Escribano, A., Regadío, M., Turrero, M.J.,
 496 2016. Lime mortar-compacted bentonite magnetite interfaces: An experimental study
 497 focused on the understanding of the EBS long-term performance for high-level nuclear
 498 waste isolation DGR concept. Applied Clay Science 124-125, 79–93.
 499 doi:10.1016/j.clay.2016.01.043

500 Dauzères, A., Achiedo, G., Nied, D., Bernard, E., Alahrache, S., Lothenbach, B., 2016.
 501 Magnesium perturbation in low-pH concretes placed in clayey environment solid
 502 characterizations and modeling. Cement and Concrete Research 79, 137–150.
 503 doi:10.1016/j.cemconres.2015.09.002

504 Dauzères, A., Bescop, P.L., Cau-Dit-Coumes, C., Brunet, F., Bourbon, X., Timonen, J.,
 505 Voutilainen, M., Chomat, L., Sardini, P., 2014. On the physico-chemical evolution of low-
 506 pH and CEM I cement pastes interacting with Callovo-Oxfordian pore water under its in
 507 situ CO₂ partial pressure. Cement and Concrete Research 58, 76–88.
 508 doi:10.1016/j.cemconres.2014.01.010

509 Fernández, A.M., Baeyens, B., Bradbury, M., Rivas, P., 2004. Analysis of the porewater
 510 chemical composition of a Spanish compacted bentonite used in an engineered barrier.
 511 Physics and Chemistry of the Earth Parts A/B/C 29, 105–118.
 512 doi:10.1016/j.pce.2003.12.001

513 Fernández, R., Cuevas, J., Mäder, U.K., 2010. Modeling experimental results of diffusion
 514 of alkaline solutions through a compacted bentonite barrier. Cement and Concrete Research
 515 40, 1255–1264. doi:10.1016/j.cemconres.2009.09.011

516 Fernández, R., Mäder, U., Rodríguez, M., de la Villa, R.V., Cuevas, J., 2009. Alteration of
 517 compacted bentonite by diffusion of highly alkaline solutions. European Journal of
 518 Mineralogy 21, 725–735. doi:10.1127/0935-1221/2009/0021-1947

- 519 Fernández, R., Ruiz, A.I., Cuevas, J., 2016. Formation of C-A-S-H phases from the
520 interaction between concrete or cement and bentonite. *Clay Minerals* 51, 223–235.
521 doi:10.1180/claymin.2016.051.2.09
- 522 Fernández, R., Torres, E., Ruiz, A.I., Cuevas, J., Alonso, M.C., Calvo, J.L.G., Rodríguez,
523 E., Turrero, M.J., 2017. Interaction processes at the concrete-bentonite interface after 13
524 years of FEBEX-Plug operation. Part II: Bentonite contact. *Physics and Chemistry of the*
525 *Earth Parts A/B/C* 99, 49–63. doi:10.1016/j.pce.2017.01.009
- 526 Fernández, R., de la Villa, R.V., Ruiz, A.I., García, R., Cuevas, J., 2013. Precipitation of
527 chlorite-like structures during OPC porewater diffusion through compacted bentonite at
528 90C. *Applied Clay Science* 83–84, 357–367. doi:10.1016/j.clay.2013.07.021
- 529 Huertas, F.J., Carretero, P., Delgado, J., Linares, J., Samper, J., 2001. An Experimental
530 Study on the Ion-Exchange Behavior of the Smectite of Cabo de Gata (Almería Spain):
531 FEBEX Bentonite. *Journal of Colloid and Interface Science* 239, 409–416.
532 doi:10.1006/jcis.2001.7605
- 533 Jenni, A., Mäder, U., Lerouge, C., Gaboreau, S., Schwyn, B., 2014. In situ interaction
534 between different concretes and Opalinus Clay. *Physics and Chemistry of the Earth Parts*
535 *A/B/C* 70–71, 71–83. doi:10.1016/j.pce.2013.11.004
- 536 Komarneni, S., Roy, D.M., Fyfe, C.A., Kennedy, G.J., 1987. Naturally occurring 1.4 nm
537 tobermorite and synthetic jennite: Characterization by ²⁷Al and ²⁹Si MASNMR
538 spectroscopy and cation exchange properties. *Cement and Concrete Research* 17, 891–895.
539 doi:10.1016/0008-8846(87)90077-9
- 540 Lothenbach, B., Nied, D., LHôpital, E., Achiedo, G., Dauzères, A., 2015. Magnesium and
541 calcium silicate hydrates. *Cement and Concrete Research* 77, 60–68.
542 doi:10.1016/j.cemconres.2015.06.007
- 543 Madejová, J., Komadel, P., 2001. Baseline Studies of the Clay Minerals Society Source
544 Clays: Infrared Methods. *Clays and Clay Minerals* 49, 410–432.
545 doi:10.1346/ccmn.2001.0490508
- 546 Mäder, U., Jenni, A., Lerouge, C., Gaboreau, S., Miyoshi, S., Kimura, Y., Cloet, V.,
547 Fukaya, M., Claret, F., Otake, T., Shibata, M., Lothenbach, B., 2017. 5-year chemico-
548 physical evolution of concrete claystone interfaces Mont Terri rock laboratory
549 (Switzerland). *Swiss Journal of Geosciences* 110, 307–327. doi:10.1007/s00015-016-0240-
550 5
- 551 Michalski, J.R., Cuadros, J., Bishop, J.L., Darby Dyar, M., Dekov, V., Fiore, S., 2015.
552 Constraints on the crystal-chemistry of fe/mg-rich smectitic clays on mars and links to
553 global alteration trends. *Earth and Planetary Science Letters*, 427, 215–225.
554 doi:10.1016/j.epsl.2015.06.020
- 555 Ni, M., Ratner, B.D., 2008. Differentiating calcium carbonate polymorphs by surface
556 analysis techniques-an XPS and TOF-SIMS study. *Surface and Interface Analysis* 40,
557 1356–1361. doi:10.1002/sia.2904

- 558 Nied, D., Enemark-Rasmussen, K., LHopital, E., Skibsted, J., Lothenbach, B., 2016.
559 Properties of magnesium silicate hydrates (M-S-H). *Cement and Concrete Research* 79,
560 323–332. doi:10.1016/j.cemconres.2015.10.003
- 561 Roosz, C., Grangeon, S., Blanc, P., Montouillout, V., Lothenbach, B., Henocq, P., Giffaut,
562 E., Vieillard, P., Gaboreau, S., 2015. Crystal structure of magnesium silicate hydrates (M-
563 S-H): The relation with 2:1 MgSi phyllosilicates. *Cement and Concrete Research* 73, 228–
564 237. doi:10.1016/j.cemconres.2015.03.014
- 565 Savage, D., Walker, C., Arthur, R., Rochelle, C., Oda, C., Takase, H., 2007. Alteration of
566 bentonite by hyperalkaline fluids: A review of the role of secondary minerals. *Physics and*
567 *Chemistry of the Earth Parts A/B/C* 32, 287–297. doi:10.1016/j.pce.2005.08.048
- 568 Turrero, M.J., Fernández, A.M., Peña, J., Sánchez, M.D., Wersin, P., Bossart, P., Sánchez,
569 M., Melón, A., Garralón, A., Yllera, A., Hernán, P., Gómez, P., 2006. Pore water
570 chemistry of a Paleogene continental mudrock in Spain and a Jurassic marine
571 mudrock in Switzerland: Sampling methods and geochemical interpretation. *Journal of*
572 *Iberian Geology* 32, 2, 233-258.
- 573 Turrero, M.J., Villar, M.V., Torres, E., Escribano, A., Cuevas, J., Fernández, R., Ruiz, A.I.,
574 de la Villa Raquel, V., de Soto, I.S., 2011. Laboratory tests at the interfaces: First results on
575 the dismantling of tests FB3 and HB4 64.
- 576 Tyagi, B., Chudasama, C.D., Jasra, R.V., 2006. Determination of structural modification in
577 acid activated montmorillonite clay by FT-IR spectroscopy. *Spectrochimica Acta Part A:*
578 *Molecular and Biomolecular Spectroscopy* 64, 273–278. doi:10.1016/j.saa.2005.07.018
- 579 Weiss, C.A., Altaner, J.S.P., Kirkpatrick, R.J., 1987. High-resolution ^{29}Si NMR
580 spectroscopy of 2:1 layer silicates: Correlations among chemical shift, structural
581 distortions, and chemical variations. *American Mineralogist* 72, 935–942.
- 582 Wypych, F., Adad, L.B., Mattoso, N., Marangon, A.A.S., Schreiner, W.H., 2005. Synthesis
583 and characterization of disordered layered silica obtained by selective leaching of
584 octahedral sheets from chrysotile and phlogopite structures. *Journal of Colloid and*
585 *Interface Science* 283, 107–112. doi:10.1016/j.jcis.2004.08.139

586

Highlights

Long-term concrete-bentonite interaction is studied in long-term experiments

Mg-silicates precipitated in bentonite at the interface with concrete

Trioctahedral Mg silicates and serpentine-type minerals are detected

Brucite intercalation in the interlayer of smectite is also detected

The Ca alkaline front from concrete is buffered by the Mg silicates formed in bentonite